

https://doi.org/10.1070/QEL16981

Confinement of electrons in the focus of the dipole wave

A.V. Bashinov, P. Kumar, E.S. Efimenko

Abstract. **Based on the numerical modelling of the electron dynamics in the focal region of a dipole wave, we have found the confinement time of electrons in the region of the strongest electric field in a wide (up to 200 PW) power range. By comparing confinement times of particles and the spatial structures of their escape, we have determined the regimes of ponderomotive escape and radiation-dominated escape corresponding to normal and anomalous radiative trapping, as well as the threshold powers of these regimes. It is shown that in the regimes of ponderomotive escape, the confinement time decreases with increasing power and stabilises at the level of one third of the wave period with the particles leaving the focal region predominantly across the electric field. In the radiation-dominated regime, the confinement time, on the contrary, increases with increasing power, the rate of transverse particles' escape decreases, and the particles leave the focal region in the form of compact beams.**

Keywords: *dipole wave, electron confinement, normal and anomalous radiative trapping.*

1. Introduction

Currently, the experiments on laser facilities with a peak power of about 10 PW [1–3] are being actively discussed and hundred-petawatt laser systems [4–6] are being designed. Along with the possibility of producing efficient sources of gamma radiation [7, 8] and initiating new photonuclear reactions [9], these facilities are expected to make significant progress in fundamental physics, in particular, in studies of the production of particle–antiparticle pairs [10].

One of the processes of the creation of matter from light relies on the concept of a quantum electrodynamic (QED) cascade [11]. When it develops in a strong laser field, electrons and positrons emit gamma photons, which, in turn, can decay into electron–positron pairs, thereby generating the next generation of photons and pairs of particles. The key parameters of the QED cascade are the field transverse with respect to the particle momentum, as well as the magnitude of the momentum itself. Optimal focusing allows one to increase these parameters at a fixed power [12, 13]. For monochromatic radiation, the strongest field in the focus can be achieved in the case of a dipole wave [14]. At the same time, the tight focusing of radiation causes a rapid escape of particles from the region of a strong field, which prevents the development of the cascade and may increase the power requirements for its initiation. Studies show that the balance of the escape and production of particles in the field of a dipole wave is reached at a power of 7.2 PW [12]. At a higher power, there occurs a vacuum breakdown, similar to the avalanche-like breakdown of gases, and the plasma density begins to grow exponentially. The vacuum breakdown is not only of fundamental interest, which opens up the possibility of studying extreme plasma states, but also can be the basis of unique sources of gamma radiation [15–17] and positron beams [18].

In addition to power optimisation, there is another important aspect, i.e. the formation of a seed for the QED cascade. In the case of tightly focused laser radiation, the target may be destroyed, and all particles can leave the region of the strong field (production region) before the radiation power reaches the level of the vacuum breakdown. To prevent this effect, targets should be optimised, for example, by selecting the appropriate concentration [19] and using substances with a high ionisation potential [20, 21]. In this case, it is necessary to know the rate at which electrons (positrons) leave the focal region in a wide range of laser powers. Particles can fall into the focus of a wave under the action of not only the leading edge of a pulse, but also a prepulse, which necessitates studies in a wide range of laser radiation powers.

If in experiments with a cascade it is necessary to ensure the presence of a substance in the focus of laser radiation, then to observe the production of electron–positron pairs from a vacuum in a field [22, 23], it is necessary to prevent the development of a cascade before the first pair is produced from a vacuum. In order to increase the amplitude of the field in the focus, it is planned to use multi-beam field configurations in such experiments [24]. In the limiting case of focusing in the form of a dipole wave, requirements to the power are significantly reduced, the latter should be hundreds of petawatts (depending on the laser wavelength), and the concentration of residual gases in the experimental chamber should be ultralow [25]. In the framework of the proposed experiment, it is necessary to exclude particles from entering the focal region. However, it is possible to soften the requirements for permissible gas concentrations by allowing particles to be in the focal region as long as the instantaneous power value is less than that required for the cascade production of pairs. To do this, one should have an idea not only about how the particles are attracted to the focus of the wave, but also about how quickly they leave this region.

A.V. Bashinov, E.S. Efimenko Institute of Applied Physics, Russian Academy of Sciences, ul. Ulyanova 46, 603950 Nizhny Novgorod, Russia; e-mail: abvk@inbox.ru;
P. Kumar Department of Physics, University of Lucknow, Lucknow-226007, India

Received 26 February 2019
Kvantovaya Elektronika **49** (4) 314–321 (2019)
Translated by I.A. Ulitkin

In addition, despite a number of studies in which peculiarities of motion in focused fields were revealed, such as the formation of electron (positron) beams [26, 27] and radiative trapping regimes [28, 29], a full-scale investigation of particle dynamics as a function of the laser beam intensity, focusing tightness and laser beam width remains relevant. Such studies will make it possible to determine in a wide range of parameters the possible regimes of particle motion and, accordingly, the threshold values of the intensities (powers) of these regimes.

This paper is devoted to the study of the dynamics of electrons and the time of their confinement at the focus of a dipole wave in a wide power range up to 200 PW, planned in the frame of the XCELS project [4]. In studies, the wavelength is $\lambda = 0.9$ μm, which also corresponds to the XCELS project. Due to the complexity of the particle motion in a standing dipole wave formed as a result of the interference of converging and diverging waves, the main research tool is numerical simulation. The simulation technique, as well as the approximations used, is described in Section 2. The results of numerical simulation and their discussion are presented in Section 3. Based on these simulations, we determine the dependence of the confinement time of particles in the focus on the power of the dipole wave. By comparing the obtained results with the analytical results in the non-relativistic limit, we show that the proposed modelling technique makes it possible to obtain a fairly accurate estimate of the confinement time of particles in the focus of the dipole wave.

In addition, we study the regimes of particle motion in the focus of a dipole wave as functions of its power and determine the threshold values of the powers for these regimes. Unlike the case of a plane wave, when it is possible to judge about the electron motion regimes by their steady-state spatial distribution, in tightly focused fields the particles quickly leave the interaction region, and the method for determining the motion regimes by steady-state spatial particle structures can lead to incorrect threshold values. In the present work, we identify the regimes of motion according to the character of the escape of particles, on the basis of which we determine their power thresholds.

2. Methods of numerical simulation

Under the action of a converging dipole wave, particles are pushed towards its focus, but their velocity is less than the speed of light. Moreover, due to the large curvature of the phase front near the focus, particles in certain parts of the trajectories can even move towards the wave, which causes them to be even more delayed relative to the wave [30]. As a result, the particles reaching the focus of the wave will interact with the standing dipole wave formed by the converging and diverging waves rather than with the converging one.

To analyse the motion of particles in a standing dipole wave, we will solve numerically the relativistic equations of motion of particles,

$$\frac{\mathrm{d}\boldsymbol{p}}{\mathrm{d}t} = -e\boldsymbol{E} - \frac{e}{mc\gamma}[\boldsymbol{pB}], \quad \frac{d\boldsymbol{R}}{dt} = \frac{p}{m\gamma}, \tag{1}$$

where $-e$ and m are the electron charge and mass; $\boldsymbol{R}$ and $\boldsymbol{p}$ is its radius vector and momentum; γ is the Lorentz factor of the electron; c is the speed of light; t is the time; and $\boldsymbol{E}$ and $\boldsymbol{B}$ are the electric and magnetic fields of a standing dipole wave, defined by relations (36) in [31].

To account for radiation losses, we use the semi-classical approximation [32]. This approximation assumes that the trajectories of particles between radiation events are classical and determined by equations (1), and the simulation of radiation losses is presented in the form of random events of photon emission according to the spectral probability density

$$\frac{\mathrm{d}W(\chi,\eta)}{\mathrm{d}\eta} = \frac{1}{\sqrt{3}\,\pi}\frac{e^2}{\hbar c}\frac{mc^2}{\hbar\omega\gamma} \times\left[\int_{\frac{2\eta}{3(1-\eta)\chi}}^{\infty} K_{5/3(y)}\mathrm{d}y + \frac{\eta^2}{1-\eta}K_{2/3}\left(\frac{2\eta}{3(1-\eta)\chi}\right)\right] \tag{2}$$

obtained in the framework of quantum electrodynamics in the constant crossed field approximation [32]. Here, η is the fraction of the electron energy carried away by the photon; $\hbar$ is the reduced Planck constant; ω is the cyclic frequency of laser radiation; K_v is the modified Bessel function of the second kind of order v; and

$$\chi = \frac{e\hbar}{m^3c^4}\sqrt{(mc\gamma\boldsymbol{E} + [\boldsymbol{pB}])^2 - (\boldsymbol{pE})^2}$$

is the quantum parameter. When a photon is emitted, the particle's momentum decreases abruptly by the magnitude of the momentum of the emitted photon. As shown by recent experiments, this approach gives the most accurate agreement between the calculation results and experimental data [33].

It should be noted that the semi-classical approximation is the most accurate in the strongly relativistic case. Nevertheless, the use of the semi-classical approximation in the weakly or even nonrelativistic case is permissible, because the radiation loss in these cases is negligible and does not have a significant effect on the particle confinement.

The numerical solution of equations (1) is based on the fourth-order Runge–Kutta method, and the Monte-Carlo method (rejection sampling) [34], which is thoroughly described in [35], is used to simulate photon emission. The production of electron–positron pairs was not taken into account, since it was not the balance of the production and escape of particles that we studied, but the time when the particles that had already been produced (or had been attracted to the focus) were in the focus.

For convenience, the origin of the coordinates was placed at the point of the greatest amplitude of the field of a standing dipole wave (centre point). Without loss of generality, it was assumed that the electric field at the centre point was directed along the z axis. The distribution of the electric field along the z axis and in the radial direction in the $z = 0$ plane is shown in Fig. 1, where the coordinate r means the distance to the z axis. Initially, the electrons were uniformly distributed inside a cylinder with a radius of 0.35λ and a height of λ. The centre of the cylinder coincided with the centre point, and the z axis was the axis of the cylinder. Below, this cylinder is used in reference to the region of the central antinode of the electric field of the dipole wave.

The shape and size of this region may be different, but it is important that it covers a significant domain of the strong field, where pairs can be produced, and also that all trapped particles near the antinode of the field are contained in the selected region, and particles trapped near the field node did not fall into it. Within the region chosen by us, the amplitude of the electric field is at least one quarter of the electric field maximum (Fig. 1), and the localised distributions of electrons, characteristic of the anomalous radiative trapping

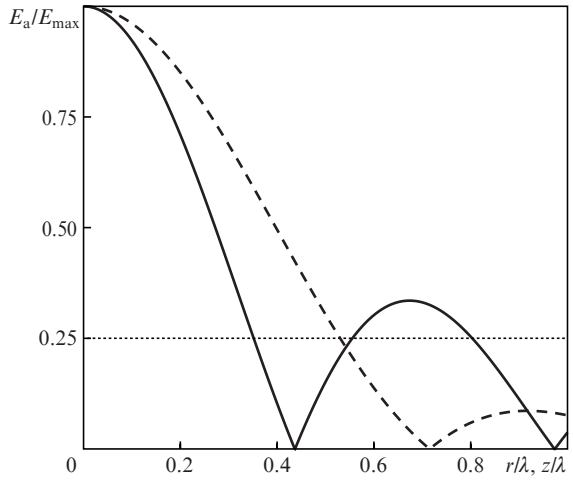

Figure 1. Distribution of the electric field amplitude E_a of the dipole wave (dashed curve) along the z axis and (solid curve) in the radial direction in the $z = 0$ plane (r axis). E_a is normalised to its maximum E_{max}. The dotted line corresponds to the level of $0.25E_{max}$.

regime [29], are inside the selected cylinder. Particles moving in the regime of normal radiative trapping [29] do not fall into the cylinder. The fact that the dipole wave has axial symmetry also speaks in favour of choosing a cylinder.

We also note that the confinement time of particles in the central antinode region depends on the field phase at which the particles begin to interact with it. In order to avoid the appearance of the constant component of the momentum, which causes a faster escape of particles, we chose the initial field phase corresponding to the largest electric and zero magnetic fields, that is, the zero vector potential. Thus, we obtain an estimate of the longest confinement time of particles in the focus.

Numerical simulation was carried out in a wide range of power (10 MW – 200 PW). The number of particles in simulations was $N_0 = 10^6$. The interaction of particles with a field was simulated for $20T$, where $T = 3$ fs is the laser field period. The time step was $0.001T$, and its further reduction did not lead to a change in the results. As shown by numerical simulation, during this time almost all particles left the region of the central antinode.

3. Discussion of the results

To determine the regimes of motion and the time of electron trapping in the focal region, we studied the change in the number of particles in the central antinode with time. Examples of the temporal dynamics of the number of particles normalised to N_0 inside the central antinode $\eta(t)$ are presented in Fig. 2 for different wave powers. $P_0 = 1$ PW is used as the unit of measurement of power, and the dimensionless power is determined by the expression $\rho = P/P_0$. The maxi-

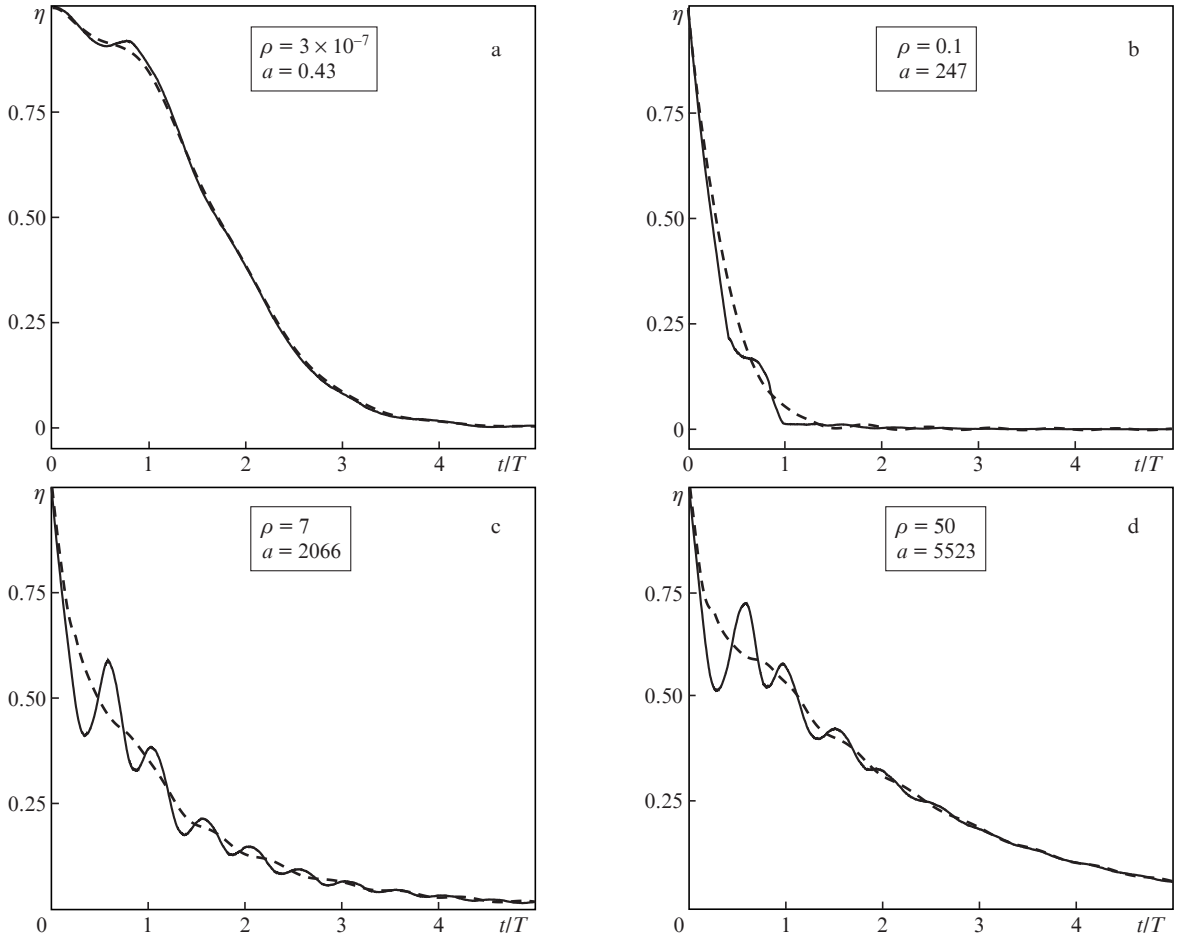

Figure 2. Temporal evolution of the number of electrons in the region of the central antinode for various dipole wave powers. The solid curve is numerical simulation data, the dashed curve is the result of smoothing the obtained data.

mum amplitude of the electric field in relativistic units a and power are related as follows [31]:

$$a = \frac{eE_{\max}}{m\omega c} = 780\sqrt{\rho}\,, \tag{3}$$

where $E_{\max}$ is the maximum electric field amplitude.

One can see from Fig. 2 that the stronger the relativistic effects of the particle motion, the more pronounced the oscillations at the doubled frequency of the laser field. Therefore, a smoothing procedure was used to average the oscillations and obtain the dynamics of the number of particles averaged over the half-period of the laser field. At the first step, a moving average approach was used with the width of the averaging window equal to the half-period of the field, as a result of which the dependence $\bar{\eta}(t)$ was obtained. At the second step, the Fourier spectrum of the difference $F(\eta(t) - \bar{\eta}(t))$ was calculated; all frequencies greater than $1.5f_0$ were rejected in the obtained spectrum, where f_0 is the frequency of the dipole wave. At the third step, the inverse Fourier transform was applied to the modified spectrum and the result was subtracted from $\bar{\eta}(t)$. As a result, we obtained the dependence of the number of particles in the central antinode on the time $\eta_{\text{av}}(t)$, averaged over the half-period of the field (dashed line in Fig. 2). It should be noted that this multi-step procedure makes it possible to suppress oscillations of $\eta(t)$ more strongly in comparison with the use of only the moving average method.

Using the results of the analysis of $\eta_{\text{av}}(t)$, for each value of the power we determined the particle confinement time $t_{1/2}$ in the region of the central antinode, at which $\eta_{\text{av}}(t_{1/2}) = 0.5$. The resulting dependence $t_{1/2}(\rho)$ is shown in Fig. 3a.

The approximation of the numerical simulation data is given below:

$$\frac{t_{1/2}}{T} = 8.9\times10^{-4}\rho^{-0.5}\sqrt{1 + 1.05\times10^{5}\rho}$$
$$= 0.7a^{-1}\sqrt{1 + 0.17a^{2}} \text{ at } \rho < 1 \text{ or } a < 780.$$

$$\frac{t_{1/2}}{T} = 0.28\exp(0.075\rho) = 0.28\exp(1.22\times10^{-7}a^{2}) \tag{4}$$
$$\text{at } 1 < \rho < 10 \text{ or } 780 < a < 2470,$$

$$\frac{t_{1/2}}{T} = 0.57\rho^{0.173} = 0.057a^{0.346} \text{ at } \rho > 10 \text{ or } a > 2470.$$

The reasoning of the form in which the approximating function was sought for at $\rho < 1$ is given in Subsections 3.1 and 3.2.

Additionally, we monitored in the calculations the direction in which the electrons escape from the focus of the wave. It was assumed that electrons that passed through the ends of the cylinder (the region of the central antinode) leave along the electric field, and those that pass through the lateral surface of the cylinder escape across it. The fractions of the total number of electrons that escaped along (η_{L}) and across (η_{T}) were counted by the time $t = 20T$ when all particles left the region of the central antinode. The dependences of the values of η_{L} and η_{T} on power are shown in Fig. 3b. By changing the character of the dependences $t_{1/2}(\rho)$, $\eta_{\text{L}}(\rho)$ and $\eta_{\text{T}}(\rho)$, we revealed various regimes of electron motion, which will be discussed below. The characteristic instantaneous electron concentration distributions in these regimes are shown in Fig. 4 in cylindrical coordinates.

3.1. Nonrelativistic case

To verify the proposed approach to determining the particle confinement time, we first consider the nonrelativistic case, when the estimate of the electron confinement time can be obtained analytically. The particle dynamics is described analytically by using the ponderomotive force [36]. As can be seen from Fig. 3b, as well as from the comparison of Figs 4a and 4e, the particles mainly escape across the electric field in the radial direction; therefore, we will neglect the displacement of electrons along the z axis. Qualitatively, such a spatial structure of the escape of electrons can be explained by the fact

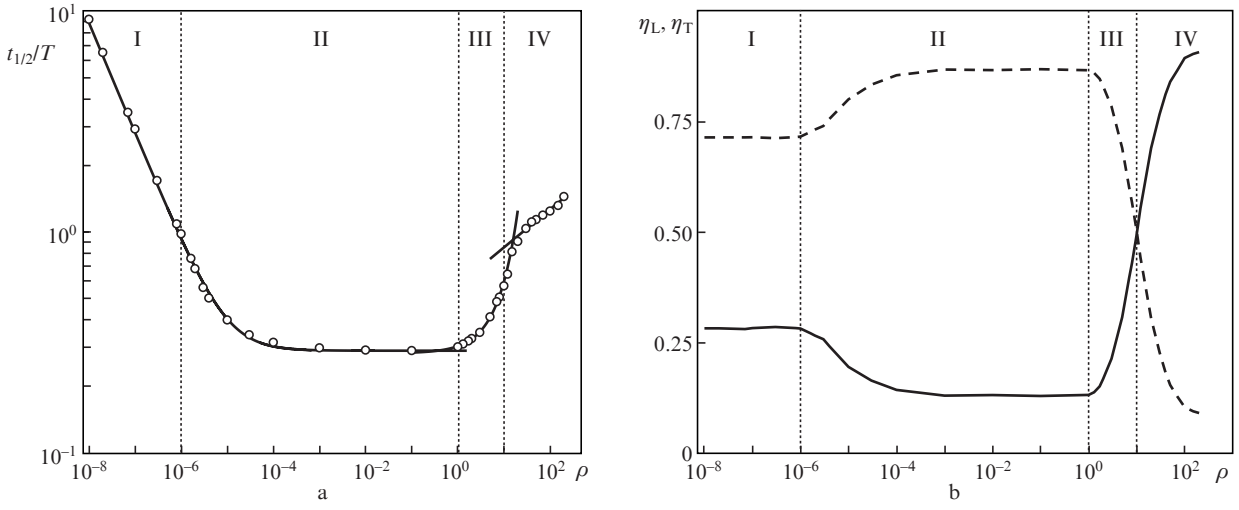

Figure 3. (a) Dependence of the electron confinement time in the region of the central antinode of a dipole wave on the power (points) and approximations of $t_{1/2}(\rho)$ in different regimes, corresponding to formula (4) (solid curves), as well as (b) dependences of the total number of electrons escaped longitudinally η_{L} (solid curve) and transversely η_{T} (dashed curve) with respect to the electric field. The vertical dashed lines separate the regions of different regimes of motion, indicated by Roman numerals.

that the radial projection of the electric field gradient exceeds the projection of the gradient on the z axis. In contrast to the case of a plane wave, when electrons oscillate in a ponderomotive potential between the antinodes of the field, in a strongle inhomogeneous field of a dipole wave particles escape from the region of the central antinode, since the neighbouring maxima of the ponderomotive potential are much less than the maximum at the centre point.

To estimate the confinement time, we consider the radial motion of an electron, initially located in the $z = 0$ plane in the vicinity of $r = 0$ (maximum of the ponderomotive potential). The averaged particle motion can be described by the following equations in cylindrical coordinates, using the ponderomotive force:

$$\frac{\mathrm{d}p_r}{\mathrm{d}t} = -\frac{e^2\partial_r E_\mathrm{a}^2}{4m\omega^2}, \quad \frac{\mathrm{d}r}{\mathrm{d}t} = \frac{p_r}{m}. \tag{5}$$

Here, p_r is the radial component of the pulse and ∂_r is the derivative with respect to r.

Let us consider the motion near the potential maximum. The electric field amplitude in this region has the following dependence on r [31]: $E_\mathrm{a} = E_\mathrm{max}(1 - 0.2k^2r^2 + O[k^4r^4])$, where $k = \omega/c$, and the linearised system of equations has the form

$$\frac{\mathrm{d}p_r}{\mathrm{d}t} = \frac{e^2E_\mathrm{max}^2 r}{5mc^2}, \quad \frac{\mathrm{d}r}{\mathrm{d}t} = \frac{p_r}{m}. \tag{6}$$

The solution to the linearised system of equations will be sought for in the form $p_r \sim r \sim \exp(\Lambda t)$. The value of Λ can be both positive and negative:

$$\Lambda_+ = -\Lambda_- = \Lambda_0 = \frac{2\pi a}{\sqrt{5}\,T}. \tag{7}$$

If we assume that the initial position of the electron is $r = r_0$ and it is at rest, then

$$r = r_0\cosh(\Lambda_0 t). \tag{8}$$

Since initially the particles are uniformly distributed inside the cylinder with a radius r_b, the decrease in the relative number of particles will be described by the expression

$$\eta = \frac{\int_0^{r_\mathrm{b}/\cosh(\Lambda_0 t)} r\mathrm{d}r}{\int_0^{r_\mathrm{b}} r\mathrm{d}r} = \frac{1}{\cosh^2(\Lambda_0 t)}. \tag{9}$$

On the basis of (9), the confinement time of particles in the region of the central antinode can be estimated as follows:

$$t_{1/2} = \Lambda_0^{-1}\mathrm{arccosh}(\sqrt{2}) \approx 0.88\Lambda_0^{-1}. \tag{10}$$

It is easy to show that in the case of a plane wave, $t_{1/2} = \Lambda_0^{-1}\mathrm{arccosh}(2) \approx 1.32\Lambda_0^{-1}$ with $\Lambda_0 = \sqrt{2}\,\pi a/T$. The smaller factor in front of Λ_0^{-1} in the case of a dipole wave is due to the fact that the farther the particles are from the z axis for the case of the initial distribution in the form of a cylinder, the greater the number of such particles. This contributes to a more rapid decrease in their number in the region of the central antinode in comparison with the case of a plane wave. In the latter case, it is natural to choose the initial distribution of particles in the form of a parallelepiped, and the number of particles in the initial distribution does not depend on their distance from the plane of the largest field amplitude.

From (7) and (10) it follows that $t_{1/2}/T \approx 0.3/a$. Thus, it can be assumed that the approximating function in the nonrelativistic limit can have the form $t_{1/2}/T = A/a$, where A is a fitting parameter. To determine the boundary value of the power (field amplitude) for the nonrelativistic case, we will make use of the numerical simulation data in Fig. 3b. Note that for $a < 0.8$ or $\rho < 10^{-6}$ (region I), the number of particles that escaped along or across the field is almost independent of power, and with increasing power it begins to change; therefore, we can use $a = 0.8$ and $\rho = 10^{-6}$ as boundary values. Then, in region I, the best fit of the approximating function to numerical simulation data is obtained at $A \approx 0.7$, which corresponds to expression (4) with $\rho \ll 10^{-6}$.

The reason for the difference between the obtained estimate and the results of the approximation can be explained as follows. First, to derive (10), we considered the motion of particles only in the $z = 0$ plane, although initially the particles are set in a fairly wide region, where the field amplitude can be 4 times less than the maximum one. Second, the description of the trajectory in the form of (8) is obtained for a small neighbourhood of the central point and is not quite true for the entire region of the central antinode. Nevertheless, it should be noted that theoretical analysis allows us to understand the type of the approximating function. In addition, if, taking into account the above reasons, we replace a by $\sim a/2$, then the analytical results and the simulation results will be quantitatively consistent. Thus, we can conclude that the proposed method for determining the particle confinement time in the central antinode region is viable.

3.2. Relativistic case

As was shown above, the threshold of the relativistic regime of motion in the problem in question is the power $\rho = 10^{-6}$ or the amplitude $a = 0.8$. According to the simulation results, in the relativistic case the confinement time is reduced (Fig. 3a) and reaches $t_{1/2} \approx 0.3T \approx L/c$, where $L \approx 0.3\lambda$ is the characteristic scale of the field inhomogeneity in the radial direction. As in the nonrelativistic case, due to the difference between the radial projection of the electric field gradient and the projection of the gradient on the z axis, most of the electrons leave the central antinode in the transverse direction (Figs 3b and 4b). At a later stage of escape ($t > t_{1/2}$), particles that have passed across the field form a quasi-cylindrical front propagating with a subluminal velocity. For the power $\rho = 0.1$, the front velocity, which is approximately determined in Fig. 4f by the surface $r = 1.4\lambda$ at the time instant $t = 1.375T$, is $0.85c$.

To select a function that approximates the simulation data, we use the results obtained by considering a similar problem in the field of a plane standing circularly polarised wave [37]. In the circularly polarised field, the exponent Λ in the relativistic case can be found by dividing the nonrelativistic expression for Λ by the Lorentz factor γ. We extend this result to the case of a standing dipole wave and look for an approximation of the data in the form $t_{1/2}/T = A\sqrt{1 + Ba^2}/a$, where A and B are fitting parameters, assuming the electron momentum $\sim amc$. Moreover, this form of the function can explain the independence of the electron confinement time at $1 \ll a < 780$ from the field amplitude (power).

To determine the boundary power of relativistic escape, we again turn to Fig. 3. The regime of particle escape begins to change qualitatively at $\rho > 1$ or $a > 780$. First, the confine-

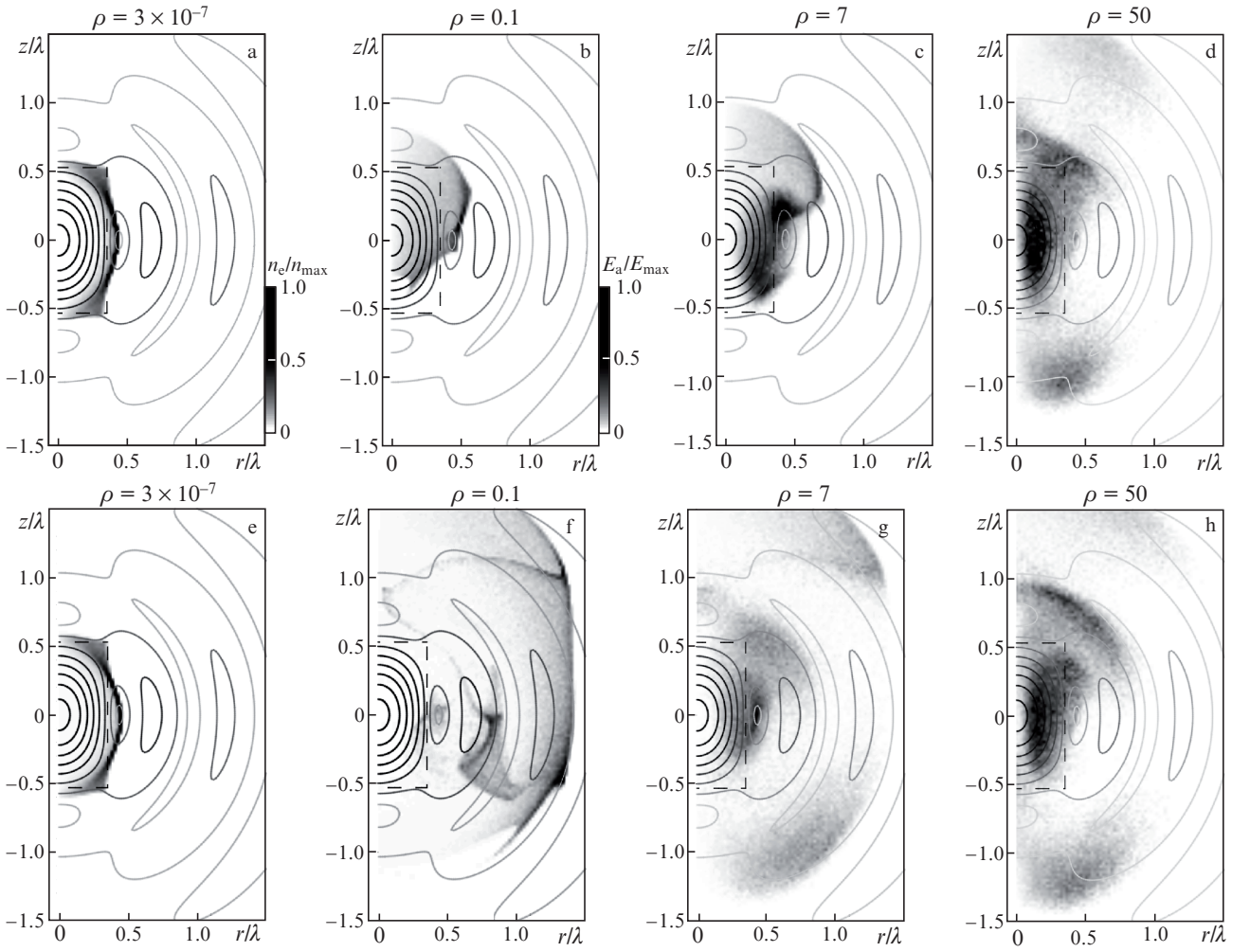

Figure 4. Electron concentration distributions n_e normalised to the maximum concentration n_{max} as functions of the coordinate z and radius r at different powers of the standing dipole wave at different points in time. The distributions in Figs 4a–4d were obtained at the instants of time $t = t_{1/2}$ corresponding to the powers indicated in the figures: (a) $1.703T$, (b) $0.289T$, (c) $0.479T$ and (d) $1.175T$. The distributions in Figs 4e–4h are presented at times $t =$ (e) $1.875T$ and (f–h) $1.375T$. Level lines indicate the distribution of the electric field amplitude, and dashed lines show the boundaries of the region within which the electrons were originally located.

ment time of electrons begins to increase, and second, the escape of particles across the field decreases and their escape in the longitudinal direction increases. In this regard, we will look for fitting parameters in the power range $10^{-6} < \rho < 1$ (region II in Fig. 3). The best fit between the numerical data and the approximating function is obtained at $A = 0.7$ and $B = 0.17$. Thus, the analogy with the case of a circularly polarised wave is confirmed, since the fitting parameter A is the same in nonrelativistic and relativistic cases.

The value of B can be qualitatively explained as follows. To estimate the Lorentz factor, we may assume the square of the electron momentum to be in average $\sim 0.5(amc)^2$. We also bear in mind the fact that, as was shown in the nonrelativistic case, taking into account the size of the central antinode, it is better to use $a/2$ instead of a. As a result, we obtain $B \approx 0.125$. A qualitative explanation of the value of the parameter A was actually given on the basis of the nonrelativistic regime.

As a result, we can conclude that both considered cases in the field of a dipole wave (regimes I and II in Fig. 3) are the regimes of ponderomotive particle escape from the region of the central antinode. The similarity of these regimes also lies in the fact that in both cases the particles mainly move in the transverse direction, the fractions of particles escaping along and across the field are practically independent of power (except for the transition region at $10^{-6} < \rho < 10^{-4}$ or $0.8 < a < 8$); in addition, we can apply for them the following formula

$$t_{1/2}/T = 8.9 \times 10^{-4} \rho^{-0.5} \sqrt{1 + 1.05 \times 10^5 \rho}$$
$$= 0.7 a^{-1} \sqrt{1 + 0.17 a^2}\,.$$

The solid curve in Fig. 3a corresponding to this formula describes with high accuracy the numerical simulation data at $\rho < 1$.

3.3. Radiative trapping

Along with relativistic effects, radiation losses can significantly influence the motion of particles at high powers. It was found previously that in the field of the dipole wave, radiation losses lead to the case of normal and anomalous radiative trapping regimes, which consist in the attraction of particles mainly to a node or to an antinode of an electric field [29].

However, the amplitude thresholds (power thresholds) of these regimes have not been established. In this section, analysing the escape of particles from the central antinode region, we not only determine the time of particle confinement, but also offer an estimate of the threshold power of the radiative trapping regimes. Unlike the case of a plane wave, in which these regimes can be analysed on the basis of the steady-state spatial distribution of particles, in the field of a dipole wave particles quite quickly leave the focal region, and this method is difficult to apply. At the same time, the power dependences of the particle confinement time and the spatial structure of their escape are different, and they can be used to determine the amplitude thresholds of the regimes.

As can be seen from Fig. 3, the relativistic regimes changes at $\rho > 1$ or $a > 780$. With increasing power, the number of particles escaping in the transverse direction decreases. Particles that have not yet left the central antinode region are grouped into a compact bunch (Figs 4c and 4d); as a result, the electrons leave this region in the form of beams (Figs 4h and 4g). Part of the particles is also trapped in the vicinity of the electric field node located at point $r = 0.44\lambda$, $z = 0$. The reason for such changes is the strong recoil resulting from the emission of photons; the strength of this recoil increases with increasing power. In the ultrarelativistic case, particles emit photons almost along the direction of their motion. The motion becomes strongly dissipative and the phase space contraction takes place, which explains the grouping of particles both inside the central antinode and in the vicinity of the field node. This regime of particles' escape can be called radiation-dominated.

Based on the properties of the dependences $t_{1/2}(\rho)$, $\eta_L(\rho)$ and $\eta_T(\rho)$, we can distinguish two regimes of radiation-dominated particle escape. The range $1 < \rho < 10$ ($780 < a < 2470$) is characterised by normal radiative trapping: most particles escape in the transverse direction (region III in Fig. 3b) and a considerable part of them is trapped in the vicinity of the field node (Fig. 4g). The word 'normal' is used in connection with the fact that the trapping is expected to occur at a minimum of the ponderomotive potential. Note that in a plane wave this regime is realised starting from a slightly weaker field ($a \approx 600$) [29]. An increase in the amplitude threshold of the regime in the case of a dipole wave can be explained by a significant difference between the amplitudes of the central and neighbouring maxima of the ponderomotive potential. As a result, the particles are most likely to overcome the neighbouring potential maximum, rather than stop and be trapped in the vicinity of the field node. This requires larger radiation losses and, consequently, larger wave amplitudes. Approximately, in this power range, the particle confinement time can be described by the exponential function (4).

At approximately $\rho \approx 10$ ($a \approx 2470$), the exponential dependence $t_{1/2}(\rho)$ changes to a power law [formula (4)], the second derivative changes its sign, and the particles begin to escape mainly along the electric field (region IV in Fig. 3b). Despite the large radial projection of the electric field gradient in comparison with the projection on the z axis, due to radiation effects the particles practically stop moving across the field at $\rho \gg 10$. Unlike the case of a plane wave, attractors in the field of a dipole wave do not form due to strong field inhomogeneity, but the regime of motion for $\rho > 10$ can be called anomalous radiative trapping by analogy. First, the probability of particle trapping in the vicinity of field node, i.e. the potential minimum, decreases significantly as the wave power increases. Second, an increase in power results in grouping of particles closer to the field antinode, i.e. the potential maximum (cf. Figs 4c and 4d), and in an increase in duration of particle motion in its vicinity. Note that, due to a significant decrease in the number of particles escaping in the transverse direction, particle beams in the anomalous trapping regime fly out of the focal area at a smaller angle to the z axis than in the case of the normal trapping regime (cf. Fig. 4g and 4h).

4. Conclusions

We have considered in a wide range of laser radiation powers the dynamics of particles in the central antinode region in the field of a dipole wave. Using numerical modelling and qualitative estimates, we have identified several regimes of motion, which differ in the characteristic confinement times of particles and the behaviour of the escape of electrons.

The first regime corresponds to the ponderomotive particle escape. In this regime, their escape occurs predominantly in the direction transverse to the electric field, since the radial projection of the electric field gradient is greatest. If, in the nonrelativistic case, the particle confinement time in the central antinode region is inversely proportional to the root of the power and its minimum value roughly corresponds to the laser field period at 1 GW, then in the relativistic case, the confinement time is determined by the ratio of the smallest scale of the spatial inhomogeneity of the field to the speed of light and is approximately equal to 1/3 of the laser period in the power range from 10 GW to 1 PW.

The second regime can be characterised as radiation-dominated particle escape. This regime arises in ultraintense fields due to strong radiation losses, as a result of which the confinement time increases and, despite the large radial projection of the field gradient, the escape of particles in the transverse direction slows down significantly. Though attractors are not formed and the particles leave sooner or later the region of the central antinode, the particles that have not yet escaped are grouped into compact bunches within this region. In particular, this leads to the formation of electron beams; the greater the power, the smaller the angle to the direction of the electric field at which they escape the focal region. The radiation-dominated escape can be divided into two regimes: normal and anomalous radiative trapping. Based on the dependences of the particle confinement time in the central antinode region, as well as on the spatial structure of the particle escape, we have determined their threshold powers to be 1 and 10 PW, respectively.

With powers of 1–10 PW, the particle confinement time begins to increase exponentially and reaches approximately 0.7 of the laser period. In this power range, most particles escape in the transverse direction of the field and most of them are grouped at the nodes of the electric field,. This corresponds to normal radiative trapping regime.

At powers above 10 PW, the regime of anomalous radiative trapping is realised. The main fraction of particles escapes in the longitudinal direction. In this case, the probability of the trapping of a particle in the vicinity of the field node significantly decreases. Particles are grouped mainly near the antinode of the field, that is, the maximum of the ponderomotive potential, and with increasing power they spend more and more time in its vicinity. In this regime, the confinement time of particles in the region of the central antinode increases according to a power law and reaches approximately 1.5 of the laser period at a power of 200 PW.

The obtained data on the confinement time of electrons in the region of the central antinode in a wide range of dipole wave powers can be used to optimise the parameters of the medium both to initiate QED cascades and to prevent their development. This may be especially important for gaseous media, when it is necessary to consider large regions of space, from where particles can fall into the focus of a dipole wave, and when three-dimensional modelling by the particle-in-cell method can become difficult.

Acknowledgements. This work was supported by the Russian Foundation for Basic Research (Grant No. 17-52-45092) and the Presidium of the Russian Academy of Sciences (Programme 'Extreme Light Fields and Their Interaction with Matter', Project No. 007-03-2018-440). Numerical simulation was carried out on the high-performance computing systems MVS-100k and MVS-10P at the Joint Supercomputer Center of the Russian Academy of Sciences.

References

1. ELI: www.eli-laser.eu.
2. VULCAN: www.clf.stfc.ac.uk/CLF/Facilities/Vulcan/.
3. Apollon: www.lcf.institutoptique.fr/lcf-en/Researchgroups/Lasers/Research-Topics/Apollon-10-PW-facility.
4. XCELS: www.xcels.iapras.ru.
5. Kawanaka J., Tsubakimoto K., Yoshida H., Fujioka K., Fujimoto Y., Tokita S., Jitsuno T., Miyanaga N., Team G.-E. D. *J. Phys. Conf. Ser*., **688**, 012044 (2016).
6. SEL: www.sciencemag.org/news/2018/01/physicists-are-planning-build-lasers-so-powerful-they-could-rip-apart-empty-space.
7. Ridgers C., Brady C.S., Duclous R., Kirk J.G., Bennett K., Arber T.D., Robinson A.P.L., Bell A.R. *Phys. Rev. Lett*., **108**, 165006 (2012).
8. Nerush E.N., Kostyukov I.Yu., Ji L., Pukhov A. *Phys. Plasmas*, **21**, 013109 (2014).
9. Thirolf P., Habs D. *Eur. Phys. J. Special Topics*, **223**, 1213 (2014).
10. Di Piazza A., Muller C., Hatsagortsyan K.Z., Keitel C.H. *Rev. Mod. Phys*., **84**, 1177 (2012).
11. Bell A.R., Kirk J.G. *Phys. Rev. Lett*., **101**, 200403 (2008).
12. Gonoskov A., Bashinov A., Bastrakov S., Efimenko E., Ilderton A., Kim A., Marklund M., Meyerov I., Muraviev A., Sergeev A. *Phys. Rev. X*, **7**, 041003 (2017).
13. Gelfer E.G., Mironov A.A., Fedotov A.M., Bashmakov V.F., Nerush E.N., Kostyukov I.Yu., Narozhny N.B. *Phys. Rev. A*, **92**, 022113 (2015).
14. Bassett I.M. *Opt. Acta*, **33**, 279 (1986).
15. Bashinov A.V., Efimenko E.S., Gonoskov A.A., Korzhimanov A.V., Muraviev A.A., Kim A.V., Sergeev A.M. *J. Opt*., **19**, 114012 (2017).
16. Jirka M., Klimo O., Bulanov S.V., Esirkepov T.Zh., Gelfer E., Bulanov S.S., Weber S., Korn G. *Phys. Rev. E*, **93**, 023207 (2016).
17. Grismayer T., Vranic M., Martins J.L., Fonseca R.A., Silva L.O. *Phys. Plasmas*, **23**, 056706 (2016).
18. Zhu X.-L., Yu T.-P., Sheng Z.-M., Yin Y., Turcu I.C.E., Pukhov A. *Nat. Commun*., **7**, 13686 (2016).
19. Jirka M., Klimo O., Vranic M., Weber S., Korn G. *Sci. Rep*., **7**, 15302 (2017).
20. Artemenko I.I., Kostyukov I.Yu. *Phys. Rev. A*, **96**, 032106 (2017).
21. Tamburini M., Di Piazza A., Keitel C.H. *Sci. Rep*., **7**, 5694 (2017).
22. Fedotov A.M., Narozhny N.B., Mourou G., Korn G. *Phys. Rev. Lett*., **105**, 080402 (2010).
23. Bulanov S.S., Esirkepov T.Zh., Thomas A.G.R., Koga J.K., Bulanov S.V. *Phys. Rev. Lett*., **105**, 220407 (2010).
24. Bulanov S.S., Mur V.D., Narozhny N.B., Nees J., Popov V.S. *Phys. Rev. Lett*., **104**, 220404 (2010).
25. Gonoskov A., Gonoskov I., Harvey C., Ilderton A., Kim A., Marklund M., Mourou G., Sergeev A. *Phys. Rev. Lett*., **111**, 060404 (2013).
26. Efimenko E.S., Bashinov A.V., Bastrakov S.I., Gonoskov A.A., Muarviev A.A., Meyerov I.B., Kim A.V., Sergeev A.M. *Sci. Rep*., **8**, 2329 (2018).
27. Luo W., Liu W.-Y., Yuan T., Chen M., Yu J.-Y., Li F.-Y., Del Sorbo D., Ridgers C.P., Sheng Z.-M. *Sci. Rep*., **8**, 8400 (2018).
28. Lehmann G., Spatschek K.H. *Phys. Rev. E*, **85**, 056412 (2012).
29. Gonoskov A., Bashinov A., Gonoskov I., Harvey C., Ilderton A., Kim A., Marklund M., Mourou G., Sergeev A. *Phys. Rev. Lett*., **113**, 014801 (2014).
30. Bashinov A.V., Gonoskov A.A., Kim A.V., Marklund M., Mourou G., Sergeev A.M. *Quantum Electron*., **43**, 291 (2013) [*Kvantovaya Elektron*., **43**, 291 (2013)].
31. Gonoskov I., Aiello A., Heugel S., Leuchs G. *Phys. Rev. A*, **86**, 053836 (2012).
32. Bayer V.N., Katkov V.M., Fadin V.S. *Izluchenie relyativistskikh elektronov* (Radiation of Relativistic Electrons) (Moscow: Atomizdat, 1973) p. 137.
33. Wistisen T.N., Di Piazza A., Knudsen H.V., Uggerhoj U.I. *Nat. Commun*., **9**, 795 (2018).
34. Neal R. *Ann. Statist*., **31**, 705 (2003).
35. Bashinov A.V., Kim A.V., Sergeev A.M. *Phys. Rev. E*, **92**, 043105 (2015).
36. Gaponov A.V., Miller M.A. *Sov. Phys. JETP*, **7**, 168 (1958) [*Zh. Eksp. Teor. Fiz*., **34**, 242 (1958)].
37. Bashinov A.V., Kumar P., Kim A.V. *Phys. Rev. A*, **95**, 042127 (2017).